

A Ripple Theorem

for Dc-to-Dc Converters Operating in Continuous Conduction Mode

*by Dr. Vatché Vorpérian
Jet Propulsion Laboratory
California Institute of Technology
Pasadena, California*

It is well known that the switching ripple information is lost in a linearized average model of a PWM converter. In this work it is shown that the switching ripple component of any state in a PWM dc-to-dc converter operating in continuous conduction mode can be recovered with remarkable accuracy from the linearized, average, small-signal model of the converter by replacing the duty-ratio control signal, \hat{d} , with the ac component of the switching PWM drive signal, $\tilde{D}_s(t) - D$, in the control-to-state transfer function. The theorem is very useful for estimating the peak-to-peak ripple in any state of a converter and is used here to determine, for the first time, the actual ripple in the zero-ripple, coupled Cuk converter as a function of the load.

The determination of the steady-state ripple current in an inductor in a dc-to-dc converter is a fairly simple task that is easily accomplished by balancing the flux in the inductor while ignoring at first the ripple voltage across the capacitor(s). Later, the ripple voltage across a capacitor is determined assuming the entire ripple current is absorbed by the capacitor.

When this simplistic approach is applied to converters with coupled inductors, such as the Cuk [1] converter or any of its derivatives, the ripple current in the inductor is shown to vanish when the coupling coefficient of the two inductors is set equal to their turns ratio. Such converters have been referred to as zero-ripple converters even though, when ideal components are used, the ripple current does not vanish.

The determination of the ripple current in such converters under zero-ripple condition has not been presented before and has sometimes been mistakenly attributed to non-ideal components. In this paper, it is observed that there is an interesting relationship between the ripple component of a voltage or current in a PWM converter, operating in continuous conduction mode, and the small-signal transfer function relating the duty-ratio control signal, \hat{d} , to that voltage or current.

Because of its generality, this observation is formulated in terms of a theorem and two corollaries. A simple proof, using the model of the PWM switch, is given. The theorem is particularly useful for analytically determining the peak-to-peak value of a ripple voltage or current and is easy to implement in circuit simulation programs.

A RIPPLE THEOREM

Some definitions are reviewed before presenting the theorem.

The steady-state (non-modulated) switching signal, $\tilde{D}_s(t)$, is the normalized drive signal applied to the gate of the active switch and is shown in Fig. 1a. The steady-state duty-ratio, D , is the dc component of $\tilde{D}_s(t)$, and $\tilde{D}'_s(t)$ is the ac component of $\tilde{D}_s(t)$, which is shown in Fig. 1b and defined as:

$$\tilde{D}'_s(t) = \tilde{D}_s(t) - D \quad (1)$$

When the switching drive signal is modulated, a low-frequency sideband accompanies the duty-ratio, D , which, in the literature of small-signal analysis, is commonly known as the control signal, \hat{d} .

Theorem: The steady-state ripple current in the switched inductor(s) in a PWM dc-to-dc converter operating in continuous conduction mode can be obtained from the average, small-signal, control-to-inductor transfer function by replacing the duty-ratio control signal, \hat{d} , with the ac component of the steady-state switching signal, $\tilde{D}'_s(t) = \tilde{D}_s(t) - D$.

Although any one of the well-known analytical methods for determining the small-signal characteristics of a dc-to-dc converter can be used to prove the theorem, we shall use the technique of the PWM switch model [2] because of its simplicity.

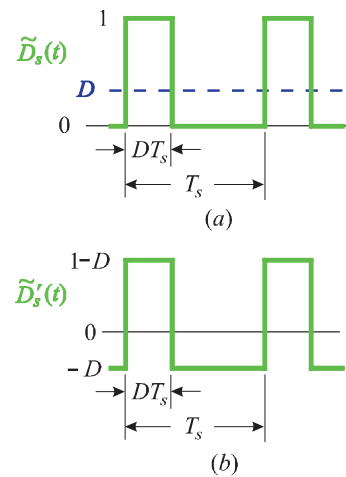


Figure 1: a) The switching signal and b) its ac component.

Proof: In all PWM dc-to-dc converters with two switched states, the voltage across the inductor and the ripple current through it have the shape shown in Fig. 2 in which the voltages V_1 and V_2 are related to the input and output voltages of the converter and satisfy the condition:

$$DV_1 = (1-D)V_2 \quad (2)$$

The effective circuit that generates the voltage and current in Fig. 2 can be configured using the PWM switch as shown in Fig. 3. In this figure we see that the dc voltage between the active and passive terminals is given by:

$$V_{ap} = V_1 + V_2 \quad (3)$$

To obtain the small-signal equivalent circuit of the circuit in Fig. 3, we set $V_1 = V_2 = 0$ and replace the PWM switch with its small-signal equivalent circuit as shown in Fig. 4.

Now, if we replace in this figure \hat{d} with $\tilde{D}'_s(t)$, the voltage across the inductor will be given by:

$$\frac{V_{ap}}{D} \tilde{D}'_s(t) D = \begin{cases} V_1 & \text{during } T_{on} \\ V_2 & \text{during } T_{off} \end{cases} \quad (4)$$

in which we have made use of Eqs. (3) and (4). Hence the small-signal model in Fig. 4, with \hat{d} replaced by $\tilde{D}'_s(t)$, generates the correct switching voltage waveform across the inductor and hence the correct ripple current through it. This concludes the proof.

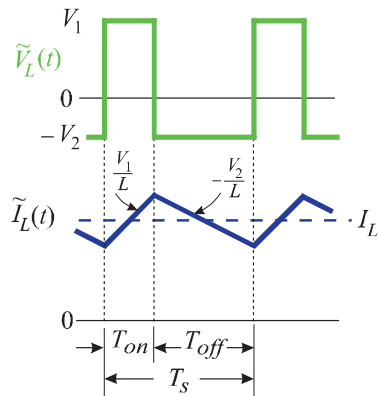


Figure 2: The voltage across a switched inductor and the current through it.

The remaining ripple components in a converter are derived either directly from the inductor ripple current (as in the case of the ripple voltage of the capacitor in the output filter of a buck converter), or indirectly from the ac component of the active terminal current (as in the case of the ripple voltage of the capacitor in the input filter of the buck converter), or from the ac component of the passive terminal current (as in the ripple voltage of the capacitor in the output filter of a boost or a buck boost converter). Hence, we compare next the active terminal current in the small-signal model in Fig. 4 and the actual circuit model in Fig. 3 in order to assess the accuracy of the switching currents obtained from the small-signal model.

From the small-signal model in Fig. 4, we see that $\tilde{I}_a(t)$ is given by:

$$\begin{aligned} \tilde{I}_a(t) \Big|_{sm_sig.} &= I_c D'_s(t) + D \tilde{I}_L(t) \\ &= I_L D'_s(t) + D \tilde{I}_L(t) \end{aligned} \quad (5a,b)$$

in which we have used $I_c = I_L$. The actual $\tilde{I}_a(t)$ from the switching circuit in Fig. 3 is given by:

$$\begin{aligned} \tilde{I}_a(t) \Big|_{actual} &= \tilde{D}_s(t)(I_L + \tilde{I}_L(t)) - D I_L \\ &= I_L D'_s(t) + \tilde{D}_s(t) \tilde{I}_L(t) \end{aligned} \quad (6a,b)$$

These two currents are sketched in Figs. 5a, b and c for three different cases of the conduction parameter, K , which correspond to heavy, critical load and no load conditions.

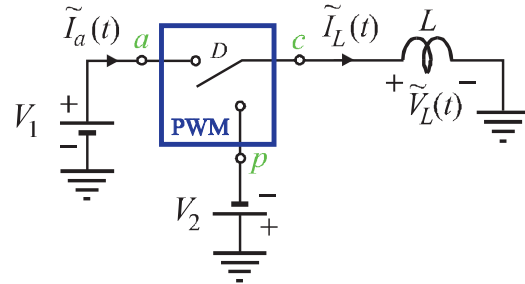


Figure 3: The effective circuit of a switched inductor using the PWM switch.

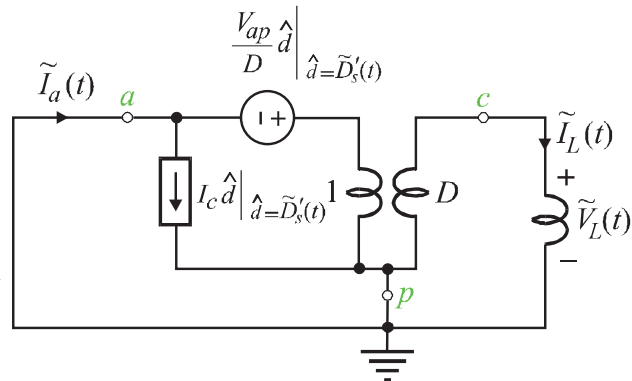


Figure 4: The small-signal equivalent circuit of the circuit in Fig. 3 using the small-signal model of the PWM.

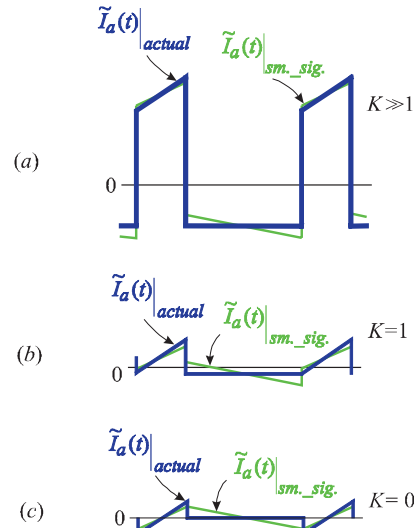


Figure 5: Comparison of the active terminal current from the actual and small-signal models in a) heavy load b) critical load and c) no load.

The conduction parameter is defined as:

$$K = 2LF_s \frac{I_c}{V_{cp}} \quad (7)$$

When synchronous rectification is not used, the critical value of $K = 1$ corresponds to boundary between continuous and discontinuous conduction modes.

It can be easily deduced from Figs. 5a, b and c that when $K \gg 1$, the actual and small models predict nearly the same switching current waveforms so that the ripple voltage induced on the capacitors which absorb these switching currents must be nearly identical in both models. When $K < 1$ however, we do not expect the shape of the induced ripple voltages in the two models to be the same, but we expect that the peak-to-peak ripple in both models to be very close because the average value of the active and passive terminal currents in each sub-interval is the same in both models. We can now state the following two corollaries.

Corollary 1: For values of the conduction parameter greater than unity, the ripple component of any state in a PWM converter can be calculated from the small-signal control-to-state transfer function, $G_{xd}(s)$, according to:

$$\tilde{X}_r(t) \approx g_{xd}(t) \circ \tilde{D}'_s(t) \quad (8)$$

in

which:

$$g_{xd}(t) = \mathcal{L}^{-1} \{G_{xd}(s)\} \quad (9a,b)$$

$$G_{xd}(s) \equiv \frac{\hat{x}(s)}{\hat{d}(s)}$$

Often, it is the peak-to-peak ripple and not its exact shape that is of interest to a designer. Hence, regardless of the value of K , the peak-to-peak ripple can be obtained to a very good approximation from the magnitude response of $G_{xd}(s)$ to the fundamental component of $\tilde{D}'_s(t)$ which is given by:

$$\frac{\sin \pi D}{\pi D} \quad (10)$$

Corollary 2: The peak-to-peak value of the ripple component in a state can be obtained, to a very good approximation, from the magnitude response of the control-to-state transfer function evaluated at the switching frequency, F_s , according to:

$$X_{r_p-p} \approx |G_{xd}(j2\pi F_s)| \frac{\sin \pi D}{\pi D} \quad (11)$$

RIPPLE ANALYSIS OF THE ZERO-RIPPLE, COUPLED CUK CONVERTER

The ripple theorem is now applied to the coupled Cuk converter [2], with a synchronous rectifier, shown in Fig. 6. The current ripple steering properties of this converter from the output inductor to the input inductor and vice-versa as a function of the coupling coefficient are well known. For the converter in Fig. 6, the triangular ripple current in the output inductor can be steered to the input inductor by letting $n = k$ which is known as the zero-ripple condition. Although in comparison to the uncoupled case the ripple current in the output inductor under zero-ripple conditions is far less, it is not zero. We shall now determine, for the first time since the introduction of this converter, the actual output ripple current and ripple voltage when the zero-ripple condition is satisfied.

The small-signal model of the Cuk converter using the model of the PWM switch is shown in Fig. 7 in which the parameters of the PWM switch are defined as:

$$\begin{aligned} V_{ap} &\equiv \text{dc voltage across port } a-p \\ I_c &\equiv \text{dc current through terminal } c \\ D &\equiv \text{duty - cycle} \\ r_c &\equiv Dr_t + D'r_d \\ D' &= 1 - D \\ r_t &\equiv Rds_{ON} \text{ of MOSFET switch (M1)} \\ r_d &\equiv Rds_{ON} \text{ of MOSFET synchronous rectifier (M2)} \end{aligned} \quad (12 \text{ a-g})$$

Before analyzing the small-signal circuit using the ripple theorem, a simulation is performed of the circuits in Figs. 6 and 7 as shown in Figs. 8a-c. The actual converter is simulated in Fig. 8a in which:

$$n = \sqrt{\frac{L_1}{L_2}} = \sqrt{\frac{50.0\mu\text{H}}{60.5\mu\text{H}}} = .909 = k \quad (13)$$

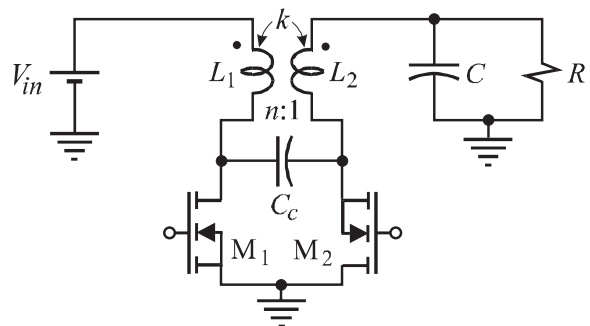


Figure 6: The coupled Cuk converter.

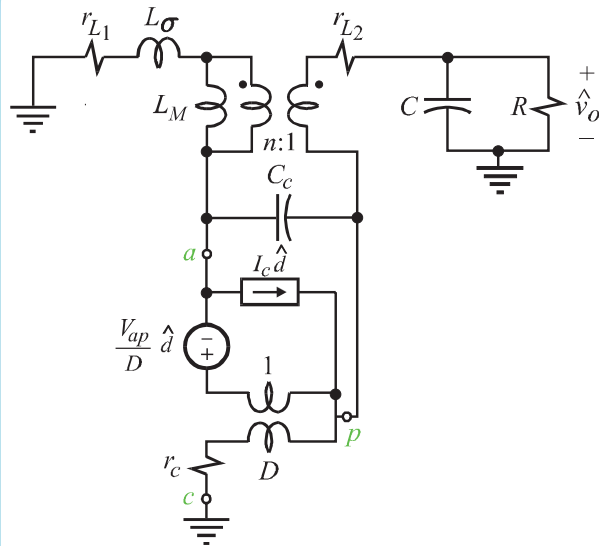


Figure 7: The small-signal equivalent circuit model of the Cuk converter using the model of the PWM switch

The gates of M1 and M2 are driven with a 5V, PWM waveform which result in an on-resistance of 150mΩ for each of the MOSFETs:

$$R_{ds_{ON}} = 150\text{m}\Omega \quad (14)$$

The small-signal equivalent circuit in Fig. 7 is simulated in Fig. 8b in which the sub-circuit U1=VMSSCCM is the small-signal model of the PWM switch in continuous conduction mode available from the ORCAD/Pspice library called *swit_rav*. The numerical values of the small-signal parameters of the PWM switch in Eqs. (12) which are supplied to VMSSCCM are shown in Fig. 8b where

$RSW = r_t = R_{ds_{ON}}$ and $RD = r_d = R_{ds_{ON}}$.

The voltage applied to terminal **Vc** is converted to the duty-ratio control signal, \hat{d} , by the Ramp parameter according to:

$$\hat{d} = \frac{V_c}{\text{Ramp}} \quad (15)$$

The default value of the Ramp is 1V. The PWM switching function, $\tilde{D}_s(t)$, and the gate-drive voltage generating circuit is shown in Fig. 8c. The ac component of the PWM switching function $\tilde{D}_s(t) - D$, is obtained at the output of the high-pass filter formed by C_x and R_x in Fig. 8b.

The results of the simulation for heavy load ($R_{load} = 5\Omega$) are shown in Figs. 9 and 10. The agreement between the small-signal model and the actual circuit is seen to be excellent for the input and output ripple currents as well as for the ripple voltages across both capacitors. It can also be seen that the output ripple current and the output ripple voltage are both non-zero even though the zero-ripple condition is satisfied. The results of the simulation for light load ($R_{load} = 500\Omega$) are shown in Figs. 11 and 12.

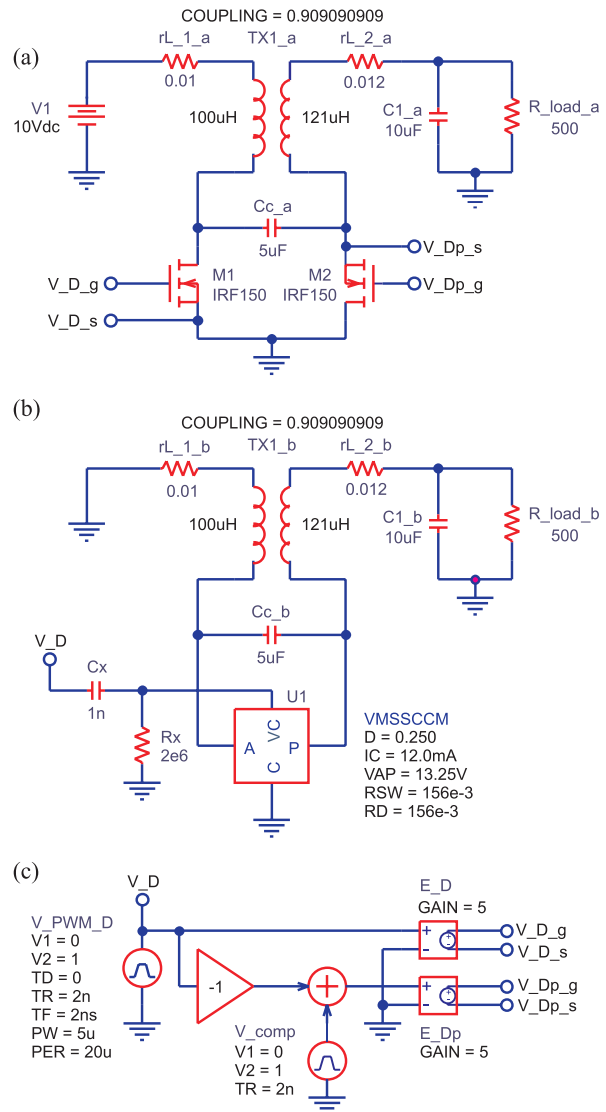


Figure 8: (a) The coupled Cuk converter, (b) the small-signal equivalent circuit model using the model of the PWM switch (VMSSCCM from the Pspice library *swit_rav*) and (c) the switching functions, $\tilde{D}_s(t)$ and $1 - \tilde{D}_s(t)$, and gate-drive signal generators E_D and E_{Dp} .

The agreement between the small-signal model and the actual circuit is seen to be fairly good especially if one is interested in determining the value of the peak-to-peak ripple. The cause of discrepancy in the small-signal result for the ripple voltage across C_c owes to the inability of the small-signal model to capture accurately the active and passive terminal currents when $K < 1$ as explained earlier in connection with Fig. 5. The excellent agreement in Fig. 11 in the input ripple current predicted by the small-signal and the actual models owes to the fact that the input ripple current, under zero-ripple conditions, mostly consists of the common-terminal current which is captured very accurately by the small-signal model. Notwithstanding these discrepancies, the usefulness of the small-signal results can clearly be appreciated.

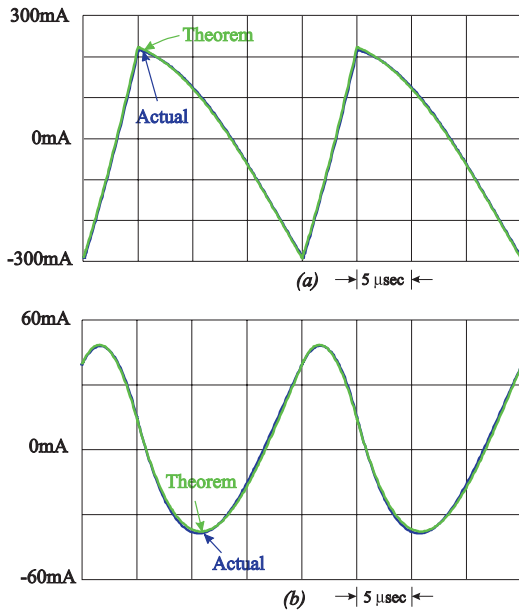


Figure 9: Comparison of the input ripple current (a) and the output ripple current (b) obtained by the theorem and the actual circuit in the coupled Cuk converter in Fig. 8 under heavy load conditions ($R_{load} = 5\Omega$) and under zero-ripple conditions.

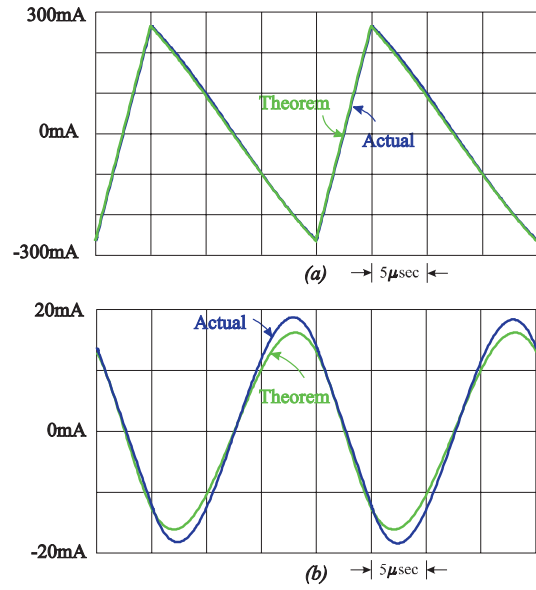


Figure 11: Comparison of the input ripple current (a) and the output ripple current (b) obtained by the theorem and the actual circuit in the coupled Cuk converter in Figs. 6 and 8a under very light load ($R_{load} = 500\Omega$) and zero-ripple conditions.

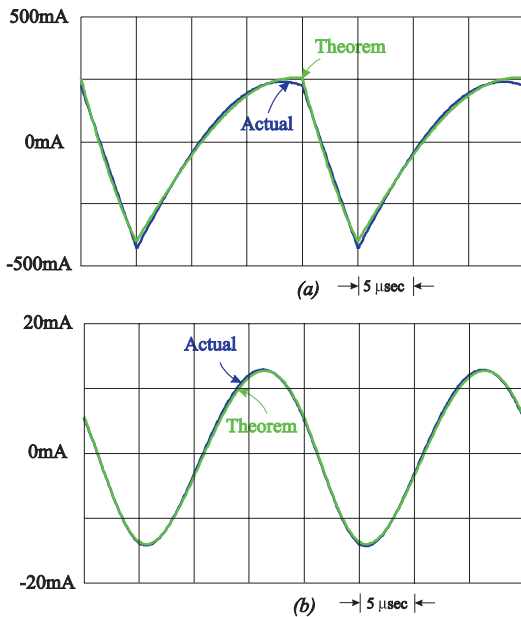


Figure 10: Comparison of the ripple voltage across C_c (a) and the output ripple voltage across C_1 (b) obtained by the theorem and the actual circuit in the coupled Cuk converter in Fig. under heavy load conditions ($R_{load} = 5\Omega$) and under zero-ripple conditions.

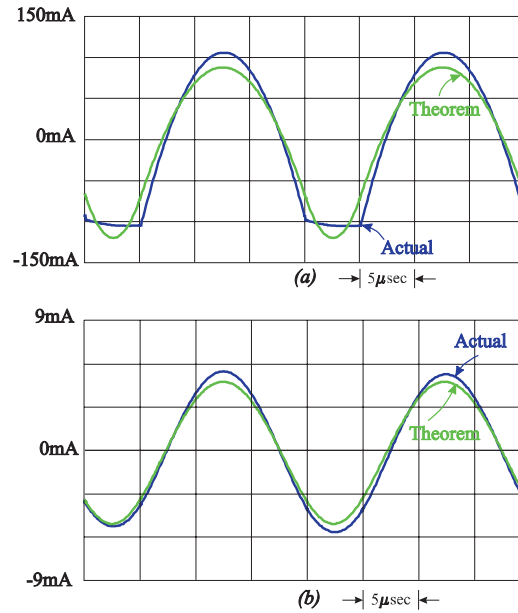


Figure 12: Comparison of the ripple voltage across C_c (a) and the output ripple voltage across C_1 (b) obtained by the theorem and the actual circuit in the coupled Cuk converter in Figs. 6 and 8a under very light load ($R_{load} = 500\Omega$) and zero-ripple conditions.

An analytical expression of the peak-to-peak output ripple voltage is obtained next from the control-to-output transfer function for heavy and light load operation under zero-ripple condition. We shall ignore the parasitic elements and deduce the control-to-output transfer function under zero-ripple condition from the results given in [3] for the isolated Cuk converter. Thus we have from [3]:

$$G_{od}(s) = \frac{\hat{v}_o}{\hat{d}} = \frac{V_o}{DD'} \frac{1-s/\omega_z}{1 + \sum_{n=1}^4 b_n s^n} \quad (16)$$

in which:

$$\begin{aligned} \omega_z &= \frac{D'^2 R}{L_1 D} \\ b_1 &= \frac{L_1}{R} \frac{D(1+D')}{D'^2} \\ b_2 &= \frac{L_1}{D'^2} [C_c + CD(1+D')] \quad (17a-e) \\ b_3 &= \frac{L_2 L_\sigma}{R} \frac{C_c}{D'^2} \\ b_4 &= \frac{L_2 L_\sigma CC_c}{D'^2} \end{aligned}$$

To evaluate the peak-to-peak ripple voltage, we do not need the complete transfer in Eq. (16). All we need to know is its behavior near the vicinity of the switching frequency. Using the numerical values of the converter, we can easily see that the denominator in Eq. (16) can be approximated by its last term in the vicinity of the switching frequency:

$$1 + \sum_{n=1}^4 b_n s^n \Big|_{s=2\pi F_s} \approx b_4 s^4 \quad (18)$$

The numerator in Eq. (16) is a function of the load so that we must evaluate it to determine the relative position of the zero with respect to the switching frequency: (19a,b)

$$\frac{\omega_z}{2\pi} = \frac{D'^2 R}{(2\pi)L_1 D} = \frac{(0.75)^2}{(2\pi)(100 \times 10^{-6} \text{H})} R = \begin{cases} 17.9 \text{kHz} & R = 5\Omega \\ 1.79 \text{MHz} & R = 500\Omega \end{cases}$$

Hence, under heavy load conditions, we see in Eq. (19a) that the RHP zero is less than the switching frequency so that the control-to-output transfer function can be approximated as:

$$G_{od}(s) \Big|_{s=2\pi F_s} \approx \frac{V_o}{DD'} \frac{-1}{s^3 \omega_z b_4} \quad ; \quad \text{heavy load} \quad (20)$$

Under very light load conditions we see in Eq. (19b) that the RHP zero is further away from the switching frequency so

that in this case the control-to-output transfer function can be approximated as:

$$G_{od}(s) \Big|_{s=2\pi F_s} \approx \frac{V_o}{DD'} \frac{1}{s^4 b_4} \quad ; \quad \text{very light load} \quad (21)$$

The peak-to-peak output ripple voltage according to Eq. (11) is given by: (22)

$$V_{r-p-p} = \begin{cases} V_o \frac{\sin \pi D}{4D'\pi^4} \frac{1}{F_s^3} \frac{1}{RCC_c L_2 (1-k^2)} & ; \quad \text{heavy load} \\ V_o \frac{D' \sin \pi D}{8D\pi^5} \frac{1}{F_s^4} \frac{1}{CC_c L_2 L_1 (1-k^2)} & ; \quad \text{very light load} \end{cases}$$

Inserting the numerical values used in the simulation in Fig. 8 we obtain:

$$V_{r-p-p} = \begin{cases} 24.6 \text{mV} & ; \quad \text{heavy load} \\ 8.8 \text{mV} & ; \quad \text{very light load} \end{cases} \quad (23)$$

These results compare well with those obtained from the simulation in Figs. 10b and 12b.

RIPPLE ANALYSIS OF THE BUCK-BOOST CONVERTER WITH AN INPUT FILTER

The ripple theorem is now applied to the buck-boost converter with an input filter shown in Fig. 13a. The small-signal equivalent circuit and the gate-drive circuit are shown in Figs. 13b and c respectively. The ripple waveforms obtained from the actual circuit are compared with those obtained from the small-signal equivalent in Figs. 14-17.

Two values of gate drive voltages are used in the actual circuit in this example. Since under light or no load conditions, the current spikes in the switches become significant in comparison to the ripple current, the gate-drive voltage is set to the low value of 5.5V which corresponds to an $r_{DS-on} = 125\text{m}\Omega$ for the IRF150. Under heavy load conditions, when $K > 1$, the gate-drive voltage is set to 8.5V which corresponds to an $r_{DS-on} = 60\text{m}\Omega$.

The ripple current in the inductor is shown in Fig. 14 under no load and full load conditions (15Ω). The agreement between the theorem and the actual waveforms is seen to be excellent. The input ripple voltage across C_{in} is shown in Fig. 15. As expected, because of the shape of the active terminal current at no load conditions, the two ripple waveforms at no load in Fig. 15a do not have the same shape but their peak-to-peak values are quite close (within 4%). The agreement is excellent however at heavy load ($R = 15\Omega$) as seen in Fig. 15b. In the same vein, the ripple current in the input filter inductor is compared in Figs. 16a and b.

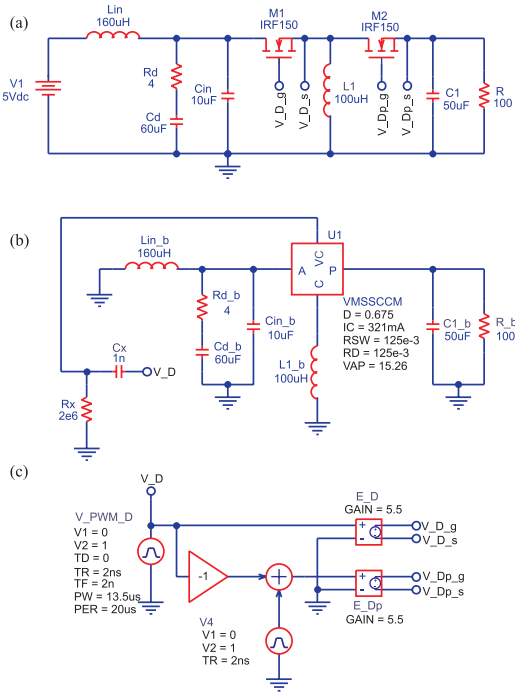


Figure 13: a) The buck boost converter with an input filter b) The small-signal equivalent circuit model and c) the gate-drive circuit.

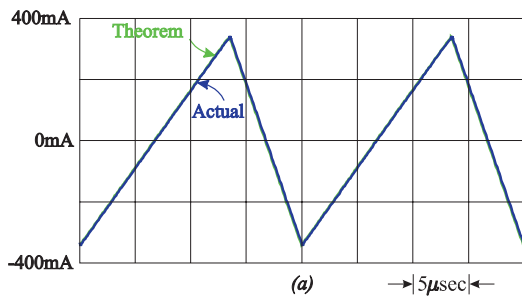


Figure 14: The inductor current at no load and R = 15W

The output voltage ripple is shown in Figs. 17a,b and c for three different values of load resistance: $R = \infty$, $R = 100\Omega$ and $R = 15\Omega$. The peak-to-peak values predicted by the theorem are in excellent agreement with those obtained from the actual circuit. The agreement in the shape of the ripple waveform improves once the load current is above the point where $K = 1$.

An important feature of the output ripple voltage in the buck-boost, or the boost converter, is that as the load current decreases, the output voltage ripple acquires a quadratic component. The ripple theorem clearly explains this effect in terms of the movement of the right-half-plane zero in the control-to-output transfer function as a function of the load current. To show this, we write the control-to-output transfer function for a simple buck-boost converter without an input filter:

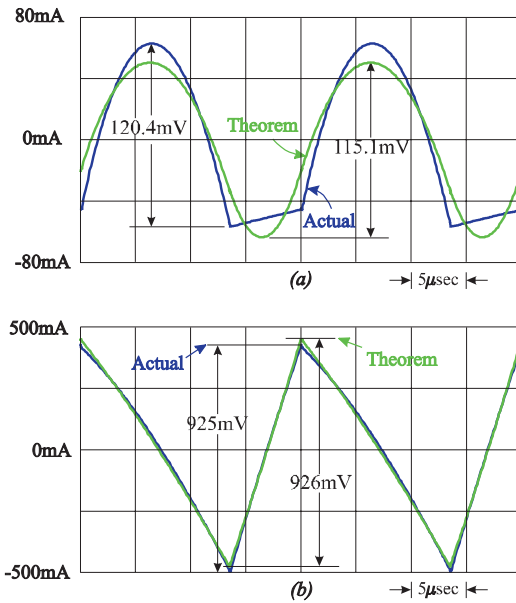


Figure 15: Input ripple voltage of the buck-boost converter a) no load and (b) $R = 15\Omega$

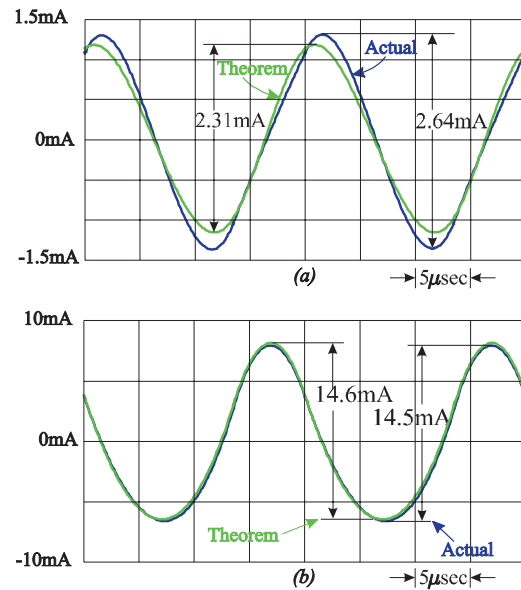


Figure 16: Input ripple current of the buck boost converter at a) no load and b) $R = 15\Omega$

$$G_{od}(s) = \frac{V_g}{D'^2} \frac{1 - s \frac{L}{R} \frac{D}{D'^2}}{1 + s \frac{L}{RD'^2} + s^2 \frac{LC}{D'^2}} \quad (24)$$

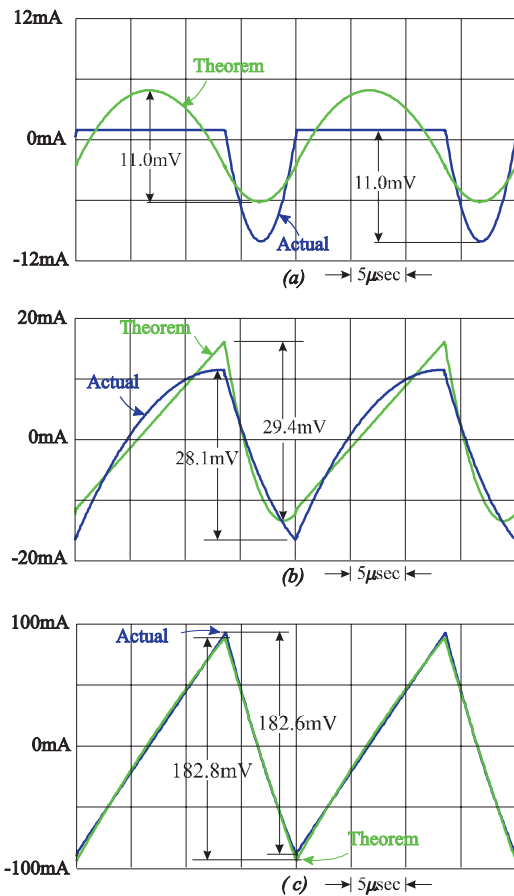


Figure 17: Output voltage ripple of the buck-boost converter for three different load conditions: a) no load, b) $R = 100\Omega$ and c) $R = 15\Omega$

In the vicinity of the switching frequency, $G_{do}(s)$ can be approximated as follows:

$$G_{od}(s) \approx \frac{V_g}{D'^2} \frac{1-s \frac{L}{R D'^2}}{s^2 \frac{LC}{D'^2}} \quad (25)$$

which in turn can be approximated for $K > 1$ and $K = 0$ (no load) as follows: (26a,b)

$$G_{od}(s) \approx \begin{cases} \frac{V_g}{D'^2} \frac{-s \frac{L}{R D'^2}}{s^2 \frac{LC}{D'^2}} = -V_g \frac{D}{sRC} & ; K > 1 \\ \frac{V_g}{D'^2} \frac{1}{s^2 \frac{LC}{D'^2}} = V_g \frac{1}{s^2 LC} & ; K = 0 \text{ (no load)} \end{cases}$$

Hence, according to Eqs. (8) and (26a,b), the ripple is proportional to the integral of $\tilde{D}'_s(t)$ under load conditions corresponding to $K > 1$ and to the double integral of $\tilde{D}'_s(t)$ (quadratic) under no load or very light load conditions. It follows that the peak-to-peak output ripple voltage is given by:

$$V_{r_{p-p}} = \begin{cases} \frac{V_o}{8} \left(\frac{f_o}{F_s} \right)^2 D'^2 & ; K = 0 \\ \frac{DI_o}{F_s C} & ; K > 1 \end{cases} \quad (27a,b)$$

in which:

$$f_o = \frac{1}{2\pi \sqrt{LC}} \quad \text{and} \quad I_o = \frac{V_o}{R} \quad (28)$$

The numerical values obtained from Eqs. (27a,b) are in excellent agreement with the values shown in Figs. 17a and c.

CONCLUSION

For PWM dc-to-dc converters operating in continuous conduction mode, a simple relationship has been uncovered between the steady-state ripple component of a state and the average, small-signal transfer function relating the duty-ratio control signal to that state. It is shown that when the duty-ratio control signal is replaced with the ac component of the PWM switching signal in any control-to-state transfer function, the steady-state ripple in that state is obtained to an excellent approximation. Since the ripple occurs at the switching frequency, it is the high-frequency behavior of the control-to-state transfer function that is closely related to the ripple component. Hence, for a given switching frequency, the attenuation in the ripple component of a state comes at the cost of either a low bandwidth or a high-order roll-off in the control-to-state transfer function. The theorem is also important to the theory of synthesis of PWM dc-to-dc converters in that it shows it is not possible to have a zero-ripple converter unless the control-to-(ripple)state transfer function vanishes.

REFERENCES

- [1] Slobodan Cuk and R.D. Middlebrook, "A new optimum topology switching dc-to-dc converter", Proceedings of the 1977 IEEE Power Electronics Conference, PESC 77 Record, pp. 160-179
- [2] Vatché Vorpérian, "Simplified analysis of PWM converters using the model of the PWM switch, Parts I and II" IEEE Transactions on Aerospace and Electronic Systems, Vol. 26, No. 3, July 1990, pp. 490-505.
- [3] Vatché Vorpérian, "The effect of the magnetizing inductance on the small-signal dynamics of the Isolated Cuk converter," IEEE Transactions on Aerospace and Electronic Systems, Vol. 32, No. 3, July 1996, 967-983.
- [4] Vatché Vorpérian, Fast Analytical Techniques in Electrical and Electronic Circuits, Cambridge University Press, 2002.

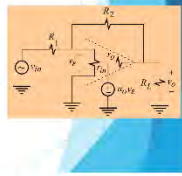
Complete Vorperian Lecture Notes

Vorperian Lecture Series Episode 1

$$\frac{R_2 a_1 R_1 r_o}{(R_1 + r_o)(R_2 r_o + R_3(r_o + R_2))}$$

gain above obtained in meaningful form:

$$1 - \frac{r_o}{a_1 R_1} \left(\frac{R_2 + R_3 + R_1 r_o}{R_1 \parallel R_2} \right)$$



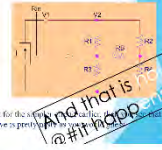
Vorperian Power Electronics Engineering

Vorperian Lecture Series Episode 2

Painful analysis of a simple bridge circuit

For a node resistance, you select for R_1 in terms of the magi Chaitin's rule:

$$\begin{bmatrix} G_1 + G_2 + G_3 & -G_3 & -G_2 \\ -G_3 & G_2 + G_3 + G_4 & -G_4 \\ -G_2 & -G_2 & -G_2 + G_4 + G_5 \end{bmatrix}$$

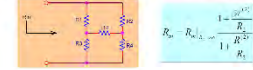


Vorperian Power Electronics Engineering

Vorperian Lecture Series Episode 3

Painless circuit analysis

Multiple meaningful solutions: For example, find the R_1 that makes the circuit...

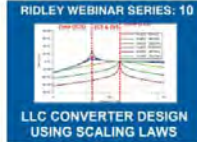


Vorperian Power Electronics Engineering

Ridley Webinar Series

LLC CONVERTER DESIGN USING SCALING LAWS

This unique presentation is by our guest speaker Nicola Rosano. The complex process of LLC converter design becomes very straightforward with the application of standardized curves combined with power and frequency scaling concepts.



MAGNETICS CORE LOSS WEBINAR

In this groundbreaking webinar, Dr. Ridley demonstrates circuit models for core loss that provide loss estimations regardless of waveform. The models provide better worst-case analysis than the original data.



HAPPY HOUR WITH DR. RIDLEY - WEBINAR

This is an open discussion without any formal presentation from Dr. Ridley. Ask any questions you like about power electronics, history, frequency response, topologies, technology, people, or the past and future of our field.

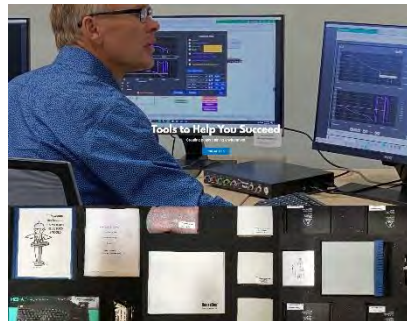


DESIGN, BUILD AND TEST A FLYBACK TRANSFORMER - WEBINAR

In this webinar Dr. Ridley shows you how to Design, Build, and Test a Flyback Transformer. We had the ambitious plan to actually build the transformer live during the webinar.



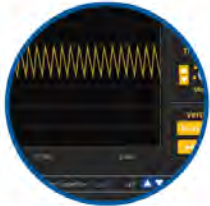
Frequency Response Analyzers



POWER
SUPPLY
DESIGN
WORKSHOP

Power Supply Design Software

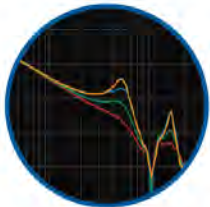




RidleyWorks® Lifetime License

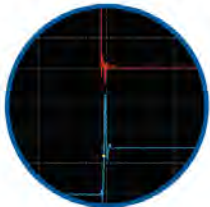
Power Stage Designer
 Power Stage Waveforms
 Magnetics Designer
 Transfer Function Bode Plots

Closed Loop Design
 Automated FRA Control
 LTspice® Automated Link
 PSIM® Automated Link



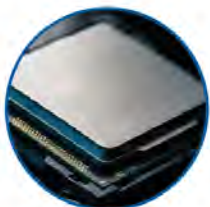
4-Channel Frequency Response Analyzer

Frequency Range 1 Hz - 20 MHz
 Source Control from 1 mV - 4 V P-P
 Built-In Injection Isolator
 Bandwidth 1 Hz - 1 kHz
 Automated Setup from RidleyWorks®
 Direct Data Flow into RidleyWorks®



4-Channel 200 MHz Oscilloscope

Picoscope® 5444D 4-Channel Oscilloscope
 200 MHz Bandwidth
 1 GS/s at 8-bit res; 62.5 MS/s at 16-bit res
 Signal Generator up to 20 MHz
 Computer Controlled



Embedded Computer

Intel® Computer with 32 GB RAM, 256 GB SSD
 Intel® HD Graphics 620
 Integrated Dual Band Wireless, Bluetooth 4.2
 Dual HDMI and USB Ports, Ethernet



Differential Probes



Line Injector



Accessories



Output Impedance



Impedance Test Kit